Using two-dimensional impedance maps to study weak scattering in sparse random media

Adam C. Luchies[a] and Michael L. Oelze
Department of Electrical and Computer Engineering, University of Illinois at Urbana-Champaign, Urbana, Illinois 61801, USA

(Received 2 March 2015; revised 5 February 2016; accepted 12 March 2016; published online 4 April 2016)

Impedance maps (ZMs) have been proposed as a tool for modeling acoustic properties of tissue microstructure. Three-dimensional (3D) ZMs are constructed from a series of adjacent histological tissue slides that have been stained to emphasize acoustic impedance structures. The power spectrum of a 3DZM can be related to the ultrasound backscatter coefficient, which can be further reduced to a form factor. The goal of this study is to demonstrate the ability to estimate form factors using two-dimensional (2D) ZMs instead of 3DZMs, which have reduced computational and financial cost. The proposed method exploits the properties of isotropic media to estimate the correlation coefficient from slices before estimating the 3D volume power spectrum. Simulated sparse collections of objects were used to study the method by comparing the results obtained using 2DZMs to those predicted by theory. 2DZM analysis was conducted on normal rabbit liver histology and compared to 3DZM analysis of the same histology. The mean percent error between effective scatterer diameter estimates from 2DZMs and 3DZMs of rabbit liver histology was $<10\%$ when using three 2DZMs. The results suggest that 2DZMs are a feasible alternative to 3DZMs when estimating form factors for sparse collections of objects. © *2016 Acoustical Society of America*.
[http://dx.doi.org/10.1121/1.4944762]

[KAW] Pages: 1557–1564

I. INTRODUCTION

Correlating histological observation with ultrasound-based estimates of scatterer properties is a common approach for studying microstructure characteristics of tissue. In early work, Fields correlated B-mode image characteristics with histological analysis in breast tumors.[1] In later work, Waag *et al.* proposed estimating the volume power spectra from the two-dimensional (2D) power spectra of optically rendered planar tissue sections for the purpose of predicting ultrasound scattering from tissues. However, in that study, the analyzed optical images were not compared to acoustic scattering predicted by theory or ultrasound measurement.[2] Insana used histological analysis of the kidney in order to select a correlation function for modeling ultrasound backscatter measurements.[3] Czarnota *et al.* observed changes in ultrasound backscatter due to cell death and correlated these changes to histological observations.[4] Mamou *et al.* constructed three-dimensional (3D) impedance maps (ZMs) from planar histology sections and compared backscatter coefficient (BSC) estimates predicted from the 3DZMs with BSC estimates from ultrasound measurements in animal models for breast cancer.[5–7] Gyöngy *et al.* simulated ultrasound B-mode images for canine mastocytoma tumors based on histology and compared the results to actual ultrasound B-mode images.[8] Of the described methods, ZM analysis has the advantage of quantitatively and directly connecting optically based histology with ultrasound measurement.

Assuming weak scattering, the 3D volume power spectrum of a 3DZM can be related to the BSC estimated from the received RF ultrasound backscatter signal.[9] Currently, 3DZMs are created from a series of adjacent histological tissue slides that have been stained to emphasize acoustic impedance structures. The slides are digitized using a camera, a realignment process is applied to the series of images, and each pixel is assigned an impedance value based on color. The impedance value images are stacked on top of each other to form a 3D computational model of acoustic impedance. In the case of an isotropic medium, the 3D power spectrum of the 3DZM can be radially averaged and related to the power spectrum of the ultrasound backscatter signal. In the case of an anisotropic medium, the ultrasound propagation direction must be known relative to the orientation of the 3DZM. The k-space line of the 3DZM power spectrum that is parallel to the ultrasound propagation direction can be extracted and related to the power spectrum of the ultrasound backscatter signal.

The process of constructing a 3DZM is expensive in terms of slide preparation time, computational time, and financial cost. A large set of histological slides need to be meticulously stained, optically scanned, and digitized. After loading the optical images to a computer, adjacent slides must be registered and aligned using a computationally intensive search over a large transformation set (i.e., rotations, translations, etc.). If the actual physical transformations experienced by the slides during ZM preparation are not included in this set, it is impossible to correctly align the slides. Sometimes slides are lost during the ZM preparation process and these missing sections must be interpolated. The

[a]Electronic mail: luchies1@illinois.edu

histology sections may take up different amounts of the applied stain, so the image colors need to be adjusted and contrast equalized. It is clear that large discontinuities can be introduced at multiple stages in the 3DZM processing pipeline, and these discontinuities can lead to distortions in the estimated power spectrum. Furthermore, large numbers of 3DZMs need to be constructed to represent a large tissue volume, such as a tumor.

The described weaknesses of the 3DZMs motivate the renewed exploration of using 2D planar sections, i.e., 2DZMs, to study BSCs. The contributions of this paper are to review the theory for studying BSCs from planar sections as originally suggested by Waag *et al.*[2] In the work by Waag *et al.*, the processing steps were applied to radially symmetric 2D power spectra having analytic expressions that could be evaluated directly in closed form and used to check results. In addition, the processing steps were applied to 2D power spectra from optical images for several media, but no comparison was completed using expected 3D power spectra. Furthermore, no guidance was offered in regard to important practical considerations when analyzing 2DZMs, such as ZM size, spacing, or slice thickness.

The contributions of the present work include numerical studies designed to quantitatively validate the 2DZM approach. Form factors were estimated using 2DZMs and compared to form factors estimated from 3DZMs. These numerical studies extend the validation provided in the study by Waag, while offering insight into practical considerations related to 2DZM analysis, including ZM size, spacing, and slice thickness. Finally, the 2DZM approach was also validated using ZMs created from excised rabbit liver.

II. THEORY

The primary goal of ZM analysis is to use optical histology to study the BSC, a quantity that is estimated from ultrasound backscatter and is a fundamental property of tissue microstructure.[10–13] When estimating the BSC using ultrasound, typically, spatial compounding is used by taking several measurements from independent tissue regions over some data block and independent BSCs are averaged to obtain an ensemble average representation. For an isotropic medium, BSC estimates from ZMs can be smoothed by using angular compounding in place of spatial compounding by radial averaging the ZM power spectrum to obtain an ensemble average representation. For an anisotropic medium, radial averaging is no longer appropriate and care must be taken to extract the correct line from the ZM power spectrum that corresponds to the ultrasound propagation direction. Note that this is true for both 3DZMs and 2DZMs.

A. Weak scattering of plane waves

Consider an infinite homogeneous medium having compressibility κ_0 and density ρ_0. In this medium, an inhomogeneity exists having compressibility and density values that vary from the infinite medium and given by $\kappa(\mathbf{r}')$ and $\rho(\mathbf{r}')$, where $\mathbf{r}'$ is used to denote a point inside the inhomogeneity. Let the smallest sphere that can be drawn to contain this inhomogeneity be labeled as V and have radius a. Define the relative compressibility and density of the inhomogeneity as

$$\gamma_\kappa(\mathbf{r}') = \frac{\kappa(\mathbf{r}') - \kappa_0}{\kappa_0} \tag{1}$$

and

$$\gamma_\rho(\mathbf{r}') = \frac{\rho(\mathbf{r}') - \rho_0}{\rho(\mathbf{r}')}, \tag{2}$$

and finally define

$$\gamma(\mathbf{r}') = \gamma_\kappa(\mathbf{r}') - \gamma_\rho(\mathbf{r}') \approx -2\frac{z(\mathbf{r}') - z_0}{z_0}, \tag{3}$$

where z is the acoustic impedance and the approximation holds when γ_κ and γ_ρ have small magnitude. Assuming plane wave propagation, weak-scattering, and that the inhomogeneity contains spatially random variations of impedance, the BSC is[14]

$$\sigma_b = \frac{k^4\langle\gamma^2\rangle}{16\pi^2}\int_{-\infty}^{\infty} b_\gamma(\mathbf{\Delta r})\exp(-j2k\hat{\mathbf{o}}\cdot\mathbf{\Delta r})\,\mathrm{d}^3\mathbf{\Delta r}, \tag{4}$$

where k is the wave number, $\mathbf{\Delta r} = \mathbf{r}_1 - \mathbf{r}_2$ is the lag vector, $\hat{\mathbf{o}}$ points in the direction of the backscattered wave, and $b_\gamma(\mathbf{\Delta r})$ is the correlation coefficient of γ. The 3D correlation coefficient is related to the BSC through the 3D Fourier transform evaluated in k-space along a line parallel to the scattered wave direction.

If the medium is isotropic, $b_\gamma(\mathbf{\Delta r}) = b_\gamma(\Delta r)$ is radially symmetric and the BSC in Eq. (4) can be simplified to[14]

$$\sigma_b = \frac{k^3\langle\gamma^2\rangle}{8\pi}\int_0^{\infty} b_\gamma(\Delta r)\sin(2k\Delta r)\,\Delta r\,\mathrm{d}\Delta r, \tag{5}$$

where the Fourier transform relationship for a 3D radially symmetric function has been used to simplify Eq. (4). The 3D volume integral in Eq. (4) has been reduced to a one-dimensional (1D) integral due to the radial symmetry of the correlation coefficient.

B. 2DZMs

If a 3DZM is available, Eq. (4) can be used to find the BSC after estimating the correlation coefficient from the 3DZM. To correctly estimate the BSC for an anisotropic medium using Eq. (4) requires knowledge of the ultrasound propagation direction relative to the ZM so that the appropriate line of the ZM power spectrum may be extracted. If 2DZMs are available, it is not possible to use Eq. (4). However, if the medium is isotropic, Eq. (5) can be used to estimate the BSC.

Isotropic random media are stationary with the additional constraint that the correlation coefficient depends on the magnitude of spatial lag (i.e., it is radially symmetric). The collection of spheres in Fig. 1(a) and the collection of randomly oriented ellipsoids in Fig. 1(b) are examples of isotropic media. Based on the properties of isotropic random media, Waag *et al.* proposed a multi-step process for

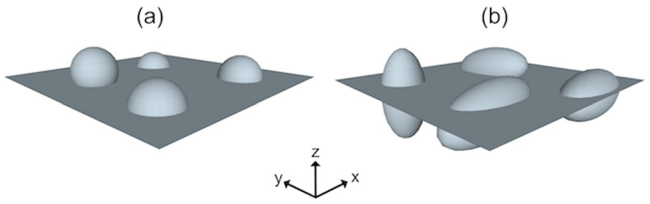

FIG. 1. (Color online) (a) Collection of randomly located spheres and (b) collection of randomly located and randomly oriented ellipsoids in isotropic media.

estimating the 3D volume power spectrum from the 2D power spectrum estimated from planar sections of the same medium.[2] The process involves converting the 2D power spectrum to a 1D power spectrum followed by conversion to a 3D power spectrum. The method requires estimation of the 2D power spectrum, numerical integration to convert to a 1D power spectrum, and numerical differentiation to convert to a 3D power spectrum.

A slightly different approach to estimating the 3D volume power spectrum from 2D slices is based on the following property of isotropic random media. An isotropic random medium in $\mathbb{R}^n$ having correlation coefficient $b(\Delta r)$ has the property that for any positive integer $m < n$ the values of this field on an arbitrary m-dimensional linear subspace form an isotropic random field with correlation coefficient $b(\Delta r)$.[15] In other words, the correlation coefficient for an isotropic 3D volume may be estimated from 2D slices. Based on this property of an isotropic random medium, the following process is proposed for estimating the BSC from 2D slices. Estimate the correlation coefficient for each 2D slice and average if more than one slice is available from the medium. In this work, the correlation coefficient for a 2DZM was estimated using

$$b(\mathbf{r}_{m,n}) = \sum_{j,k=0}^{N} \gamma\left(\mathbf{r}'_{j,k} + \mathbf{r}_{m,n}\right)\, \gamma(\mathbf{r}'_{j,k}), \tag{6}$$

where j denotes the x axis index, k denotes the y axis index, and $\mathbf{r}_{m,n}$ denotes the lag position for the mth and nth indices. Radial average the resulting 2D correlation coefficient to obtain a 1D function of lag. Substitute this correlation coefficient into Eq. (5) to estimate the BSC.

C. Evaluating measurement accuracy

For the BSC, the form factor representation $F = \sigma_b/\sigma_0$, where σ_0 is the BSC in the Rayleigh limit. The form factor was found by removing the dependence on k from the term in front of the integral in Eq. (4) and normalizing by a constant such that $F(0) = 1$, meaning the form factor is the power spectrum of the relative impedance values of the medium. To evaluate the accuracy of the form factor estimates, the mean absolute error (MAE) was used

$$\mathrm{MAE} = \frac{1}{N}\sum_{i=1}^{N} |10\, \log_{10}(F_{\mathrm{est}}(k_i)/F_{\mathrm{th}}(k_i))|, \tag{7}$$

where $F_{\mathrm{est}}(k)$ is the form factor estimated using ZMs and $F_{\mathrm{th}}(k)$ is the theoretical form factor for the medium.

III. SIMULATIONS

The primary goal of the simulation studies was to verify that 2DZMs can be used to accurately estimate form factors. In addition, the studies were designed to offer practical guidance for 2DZM analysis, including ZM size, spacing, and section thickness. 2DZMs extracted from sparse collections of simple objects, including spheres and ellipsoids, were used to estimate 3D power spectra. Because the simulated ZMs had known form factors, they could be used to determine the accuracy of using 2DZMs to estimate form factors.

Two methods were explored for improving the accuracy of using 2DZMs to estimate form factors representing 3D volumes. The first method was to increase the physical size of the 2DZM. For a typical tissue, each histological section contains many scattering object cross sections. These objects could be cells, ductal structures, nerve bundles, muscle fibers, etc. Increasing the physical size of the 2DZM increases the number of object cross sections included in the ZM analysis, leading to more accurate form factor estimates assuming that the properties of the objects in the cross section are uniform.

The second method for improving form factor estimate accuracy was to increase the number of 2DZMs that were extracted from the volume. Each 2DZM was used to independently estimate the correlation coefficient and the resulting correlation coefficients were averaged before being used to estimate the form factor. When sectioning a tissue for 3DZM analysis, the slices are successively cut from the tissue and have regular spacings, suggesting that slices extracted at regular spacings be studied for 2DZM analysis. Furthermore, analyzing 2DZMs that intersect different sets of objects as shown in Fig. 2(a) is equivalent to increasing the size of the 2DZM. Averaging correlation coefficients from slices that intersect different objects discards information about the positions of objects relative to each other. For regularly spaced slices having separation less than the object diameter, information about relative object positions will be present in the estimated correlation coefficients. Therefore, the regularly spaced slices were extracted from a layer of the volume that had thickness on the order of the size of the scattering objects as shown in Fig. 2(b). Increasing the regularly spaced slice density in this manner is different from increasing the physical size of the 2DZM, because adjacent 2DZMs have similar cross sections.

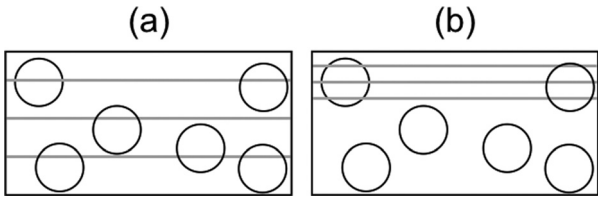

FIG. 2. 2D side view of several collections of spheres. Spheres are depicted as black circles and slices are depicted as gray lines. (a) Three regularly spaced slices having spacing greater than the sphere diameter causing the object cross sections in adjacent slices to be unrelated. (b) Three regularly spaced slices having spacing less than the sphere diameter causing the object cross sections in adjacent slices to be related.

The simulation studies were used to determine the effectiveness of the two described methods for increasing the accuracy of using 2DZM form factor estimates. Volumes containing different numbers of objects were simulated. To study the effect of physical 2DZM size on form factor estimates, the size of the simulated 2DZM was expanded to increase the number of objects included in the analysis. Initially, a single slice was extracted from the volume. To study the effect of regularly spaced slice density, the analysis was repeated using different numbers of regularly spaced slices that were drawn from a layer in the volume having the same thickness as the diameter of the objects. Therefore, each simulation volume was generated by specifying an average number of objects per slice (physical 2DZM size) and an average number of regularly spaced slices per object (regularly spaced slice density). The number of objects per slice was varied from {1,2,…,100} and the number of regularly spaced slices per object was varied from {1,3,5}. For each 2DZM size and regularly spaced slice density combination, a total of 50 simulation volumes were generated to produce 50 correlation coefficient and form factor estimates.

The simulated volumes were two-phase media, i.e., the background had a value of zero and the inside of the object had a value of one. When analyzing ZMs, the first step is to subtract the impedance value of the background medium in which the scatterers are embedded. For real ZMs that consist of sparse collections of objects, this normalization step can be accomplished by subtracting the mean value of the ZM from itself. The centers of the objects were sparsely located and had a separation distance of at least twice the diameter of the object. When estimating the correlation coefficient for the simulated ZMs, an object size, $\hat{a}$, was estimated by fitting a spherical model to the correlation coefficient. Before estimating the form factor, the correlation coefficient was set to zero outside the lag distance $0 \leq \Delta r \leq 2\hat{a}$. This restriction eliminates large lag content in the correlation coefficient and reduces the corresponding noise in the form factor estimates. The form factor was then estimated for the range $0 \leq ka \leq 4$. Usually BSCs estimated using ultrasound have their support in this range.

Collections of monodisperse spheres having radius a were simulated. A correlation coefficient was estimated for each 2DZM and then radially averaged to form a 1D function of spatial lag and used in the numerical evaluation of Eq. (5). In the case of multiple 2DZMs, a correlation coefficient was estimated for each 2DZM and the correlation coefficients were averaged to form a single 2D correlation coefficient before radial averaging. Performance was quantified using Eq. (7) by comparing the theoretical form factor for a single sphere with the 2DZM form factor estimate. The primary goal of this simulation was to study the performance of the 2DZM method assuming an isotropic medium when using different slice sizes and regularly spaced slice densities.

Simulations of monodisperse spheres are a standard example when exploring new methods for studying acoustic scattering. However, real tissues are more complex than monodiperse spheres, so it is important to examine the behavior of 2DZMs when analyzing more complex media. Collections of randomly oriented ellipsoids having radii a, $0.8a$, and $0.6a$ were simulated. The correlation coefficient and form factor were processed in the same way as for the sphere collection simulations. Performance was quantified using Eq. (7) by comparing the theoretical form factor for a collection of randomly oriented ellipsoids with the 2DZM form factor estimates.[17] The primary goal of these simulations was to study the performance of the 2DZM method for an isotropic medium having scatterers with non-spherical shape.

In addition to having non-spherical shape, the scatterers in real tissues often have varying sizes. Therefore, collections of polydisperse spheres having radii governed by a uniform distribution with minimum of $0.8a$ and maximum of $1.0a$ were simulated. The correlation coefficient and form factor were processed in the same way as for the sphere collection simulations. Performance was quantified by comparing the theoretical form factor for a collection of polydisperse spheres with the 2DZM form factor estimates.[16] The primary goal of these simulations was to study the performance of the 2DZM method for an isotropic medium having scatterers with varying sizes.

When creating histological slices from a tissue, the slides have finite thickness and this thickness affects the results of the ZM analysis. In order to study the effect of ZM slice thickness on the processing of 2DZMs, the simulations were repeated using a finite slice thickness of 10% of the object diameter (i.e., $0.2a$). The cross section was produced by extracting a 3DZM having x- and y-dimensions of the 2DZM and z-dimension equal to the slice thickness. Next, the 3DZM was projected to form a 2DZM by taking the maximum value along the z-axis. In this way, the largest radius contained in the sphere cross section was obtained. After creating 2DZMs, processing proceeded the same as with the normal sphere collection simulations. These thickness simulations were studied for spheres and randomly oriented ellipsoids.

IV. EXPERIMENTS

The 2DZM analysis procedure was tested using ZMs constructed from the livers of New Zealand white rabbits. The cell nucleus was previously suggested as a primary source of scattering in liver and also fulfills the definition of sparsity used in the present work, i.e., that scatterers be separated by one diameter. Lobes of normal liver from New Zealand white rabbits were excised, chemically fixed in formalin, sliced into 3 μm sections, stained with hematoxylin and eosin (H&E), and prepared as standard histology slides. Each slide was digitized using a NanoZoomer HT slide scanner (Hamamatsu, Hamamatsu City, Japan) at a pixel resolution of 0.46 μm.

A total of 24 3DZMs were created from the excised liver sample using previously described techniques.[7,18] Impedance values were assigned as in Pawlicki *et al.*[18] A correlation coefficient was estimated for each of the 3DZMs by first estimating the 3D correlation coefficient and radially averaging to form a 1D function of lag. For each of the 3DZMs, the correlation coefficient was estimated using

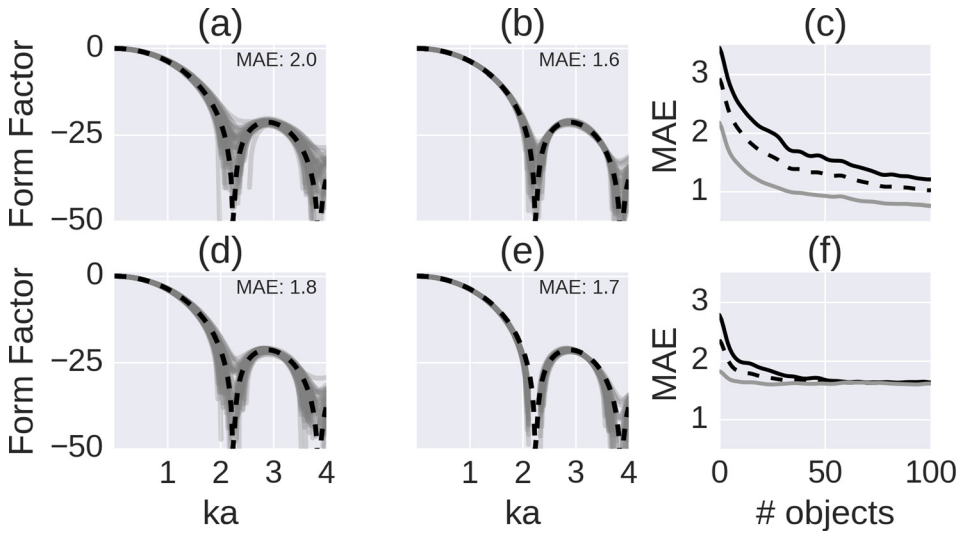

FIG. 3. (Color online) Monodisperse sphere simulations. Example form factor estimates when using [(a) and (d)] 25 object cross sections per slice and one regularly spaced slice and [(b) and (e)] 25 object cross sections per slice and 3 regularly spaced slices. Each solid gray line represents the form factor estimated from a separate simulation. The dashed black lines represent the theoretical form factor. [(c) and (f)] Average over 50 simulations of the MAE for the form factor estimated using different numbers of object cross sections per slice. The solid black, dashed black, and solid gray lines are for 1, 3, and 5 regularly spaced slices per object diameter. Top and bottom rows were using a slice thickness of 0% (i.e., a perfect cross section through the 3DZM) and 10% of object diameter (i.e., 0.2a), respectively.

different collections of 3DZM slices (i.e., 2DZMs). Collections of 3DZM slices were formed by random selection (i.e., not regularly spaced). Collections containing 1 slice, 2 slices, etc., through 25 slices were examined. For each collection of 2DZMs, the 2D correlation coefficient was estimated for each 2DZM and the resulting 2D correlation coefficients were averaged. The resulting 2D correlation coefficient was radially averaged to form a 1D function of lag.

A fluid-filled sphere correlation coefficient model was fit to the correlation coefficients and used to estimate an object size, $\hat{a}$. A form factor was estimated from each correlation coefficient using the lag range $0 \leq \Delta r \leq 2\hat{a}$. An effective scatterer diameter (ESD) based on the fluid-filled sphere model was estimated using the 3DZM and the 2DZM form factors. Percent error between scatterer sizes estimated using 3DZMs and 2DZMs was used to determine the efficacy of the 2DZM method.

V. RESULTS

A. Collection of spheres and ellipsoids

Figure 3 presents examples of estimated form factors for different configurations of object cross sections per slice, number of regularly spaced slices, and slice thickness, along with the MAE of the form factor for the sphere simulations. A total of 50 simulations for each 2DZM size and density configuration are represented. The results for the randomly aligned ellipsoid, and polydisperse sphere simulations are shown in the same format as the monodisperse sphere simulations in Figs. 4 and 5, respectively. The form factors for a randomly oriented ellipsoid collection and for a polydisperse

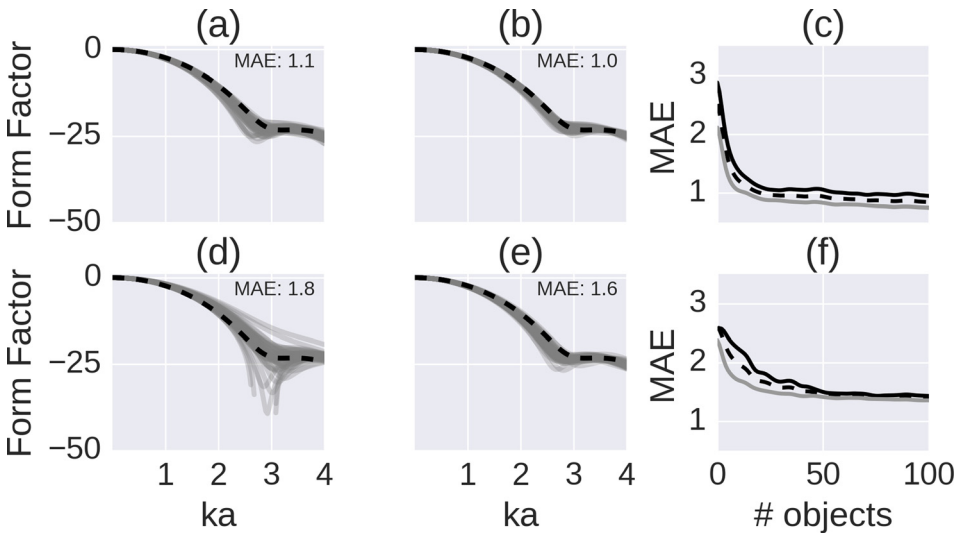

FIG. 4. (Color online) Monodisperse randomly oriented ellipsoid simulations presented in the same format as Fig. 3.

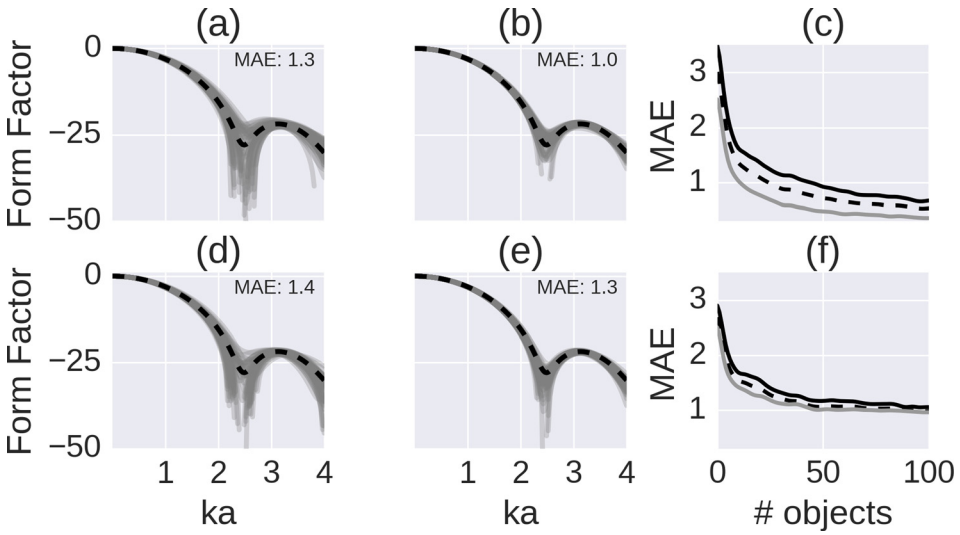

FIG. 5. (Color online) Polydisperse sphere simulations presented in the same format as Fig. 3.

sphere collection are linear combinations of sphere form factors having different sizes.

B. Experiments

Examples of form factors estimated from rabbit liver ZMs are shown in Fig. 6. The solid gray line represents the form factor estimated using a 3DZM. The solid black line represents the form factor estimated using 2DZMs. The dashed lines represent the fluid-filled sphere model fits to the solid black and gray lines. In Figs. 6(a) and 6(b), one and five 2DZMs were used to estimate the form factor, respectively.

In Fig. 6(c), the MAE is shown as a function of the number of 2DZMs used in the form factor estimate. The MAE declines rapidly in the region of 1–5 slices and then slowly in the region of 5–25 slices. For the 3DZM analysis and when using three 2DZMs, the average ESD using the fluid-filled sphere model was $6.0 \pm 0.3\,\mu$m and $6.0 \pm 0.5\,\mu$m, respectively.

VI. DISCUSSION

The simulations were conducted for collections of spheres and ellipsoids having known sizes and the results were given in terms of those sizes. In a real tissue ZM analysis, the sizes of the objects in the medium are unknown and need to be determined based on the ZM analysis. The simulation results can still be applied to guide ZM analysis of an uncharacterized medium if the first step is to use the correlation coefficient to estimate an object size, $\hat{a}$, using a spherical model as described above. The simulation results are also presented in terms of the number of object cross sections per slice. For a sparsely filled medium of discrete objects, counting the number of object cross sections per slice can be achieved through visual inspection of histology images or the ZMs themselves. For example, it is straightforward to count the number of cell nuclei in the rabbit liver histology images used in this study.

The results shown in Figs. 3–5 demonstrate that form factors can be estimated accurately using 2DZMs. To minimize form factor error, the size of the 2DZMs and regularly spaced slice density should be made as large as possible to maximize the number of object cross sections included in the analysis. However, ZM size is limited by tissue size and computational limitations. Slice density is limited by slice

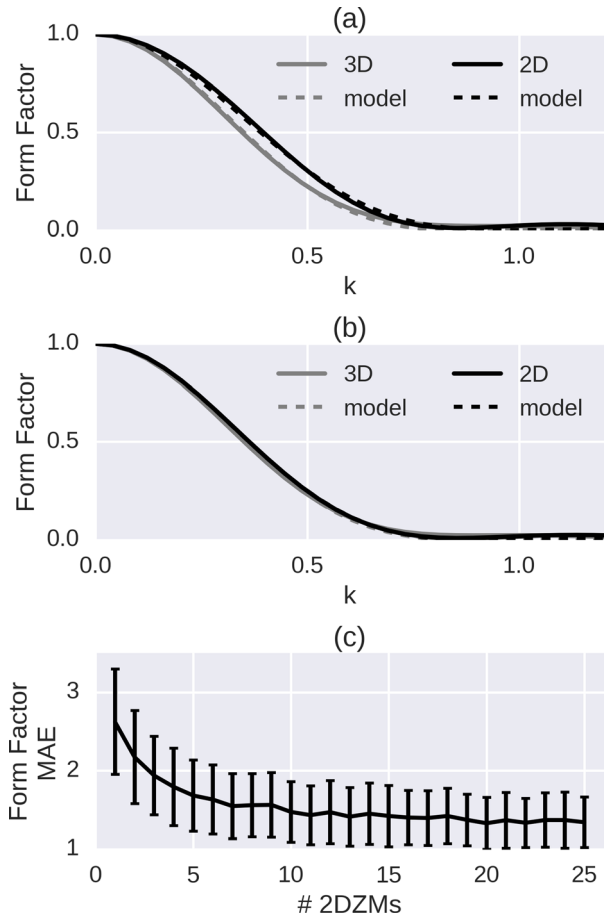

FIG. 6. (Color online) Examples of form factors estimated using a 3DZM and collections of 2DZMs from the 3DZM. (a) One and (b) five 2DZMs were used to estimate the form factor displayed as a solid black line. (a,b) One 3DZM was used to estimate the form factor displayed as a solid gray line. The dashed lines represent the fluid-filled sphere model fits to the displayed form factors. (c) MAE between form factors estimated using 3DZMs and 2DZMs for 24 samples and as a function of the number of averaged 2DZMs. Error bars represent one standard deviation.

thickness and by the financial cost of slice processing. The simulations in this study can help to assess expected error for the slice size, spacing, and thickness in a ZM analysis of real tissue.

The MAE curves presented in Figs. 3–5 show a region of rapid decline followed by a region of slow decline. Ideally, ZM analysis should occur in the region of slow decline. The division between rapid and slow decline in the MAE varied for the different simulated objects, typically occurring in the range 10–50 object cross sections per slice. For the rabbit liver histology images examined in this study, the number of cell nuclei cross sections per slice was usually in the range 70–130, suggesting that form factors for the rabbit liver would be in the slow decline region of the MAE.

The advantage of using regularly spaced slices is most pronounced for the sphere simulations. Note that increasing the regularly spaced slice density cannot be accomplished by dividing a single 2DZM into smaller regions and processing the collection of 2DZMs. The slices need to be adjacent to each other at regularly spaced intervals and from a slab of the tissue that has thickness less than the size of the objects to realize the observed reductions in error. From Figs. 3(c) and 5(c), a difference in the MAE curves of approximately 0.3 and 0.2, respectively, existed between the 1, 3, and 5 regularly spaced slices per object diameter. For the ellipsoid simulation results shown in Fig. 4(c), this difference was <0.05. This result suggests that for media filled with spherical objects, form factor estimate error may be reduced significantly using regularly spaced slices. However, Figs. 3(f) and 5(f) suggest that the advantage of using regularly spaced slices largely disappears when using slices with thickness on the order of 10% of the object diameter. In the rabbit liver studies, the slice thickness was on the order of 40% of the estimated cell nucleus diameter, suggesting that using regularly spaced slices is not efficient for reducing form factor error in the rabbit liver ZMs.

In the mondisperse sphere simulations, for the case of one slice having a size that included 50 object cross sections, the form factor MAE increased by $\sim$48% when using a slice thickness of 10% of the sphere diameter compared to a slice thickness of 0%. In addition, estimating the sphere size from the form factor produced average errors of 4% and 6% for slice thicknesses 0% and 10% of the sphere diameter, respectively. Increasing the slice thickness caused the form factor nulls to shift slightly toward the origin, which is the same as an increase in size in the spatial domain. Using a finite slice thickness causes the circle cross sections to be larger than if zero thickness slices were used, leading to a form factor with an inflated sphere size compared to the actual sphere size. Similar effects were observed for the polydisperse sphere and monodisperse ellipsoid simulations. 3DZMs are also affected by slice thickness resulting in biases in scatterer size estimates.

The rabbit liver results demonstrate that 2DZMs can be used to estimate a form factor that closely matches a form factor using a 3DZM. The reduction in ZM processing gained from the 2DZM method is clear from Fig. 6. In Fig. 6(b), 5 slices (i.e., 2DZMs) were used to estimate the dashed black line, compared to 100 slices in the 3DZM used to estimate the solid gray line. In Fig. 6(c), the MAE between the 2DZM and 3DZM estimated form factor decreased slowly in the region 5–25 slices, suggesting that averaging additional slices will lead to minor improvements in the form factor estimate.

The 3DZM has several advantages compared to the 2DZM. For isotropic media, 3DZMs provide more independent radial lines for averaging when estimating the correlation coefficient compared to using a single 2DZM. Increasing the number of independent estimates available for averaging improves form factor estimates. In addition, the 2DZM approach assumes that the scatterers in the medium are sparsely located. This limitation does not affect the 3DZM approach because the effects of the correlations between scatterer positions are included when estimating the 3DZM power spectrum using the squared modulus of the 3DZM Fourier transform. However, the 2DZM approach could be modified to take into account coherent effects that would be present in a dense medium.

In many cases, the advantages of working with 2DZMs outweigh the advantages of working with 3DZMs. For example, when the medium contains objects with different sizes (i.e., a form factor with on nulls), the simulations suggest that using a single slice with $\sim$50 object cross sections is feasible for estimating form factors from 2DZMs, while 3DZMs require hundreds of slices. Using fewer slices translates into decreased preparation time and financial cost. In addition, the registration and alignment process that is critical to the success of 3DZM analysis is unnecessary when working with 2DZMs.

When several 2DZMs are available, the correlation coefficient can be estimated for each 2DZM independently and then averaged without the need for registering and aligning the 2DZMs. Furthermore, the slice thickness for 3DZMs is not equal to the pixel width in the slice plane. This can cause artifacts in the form factor estimates. Finally, even with radial averaging, obtaining good estimates from a 3DZM requires multiple independent 3DZMs.

VII. CONCLUSION

This work proposed a method for using 2DZMs to study fundamental acoustic properties of tissues such as the BSC. Processing 2DZMs has numerous advantages compared to processing 3DZMs, including reduced computational and financial cost. The methods proposed in this work are for isotropic media, two modeling assumptions commonly used when working with weak scattering biological tissues. The simulations demonstrated the proposed methods on sparse collections of spheres and ellipsoids. The simulation results revealed that increasing the 2DZM size was effective for decreasing form factor estimate error up to a point, beyond which only minimal reductions in error were achieved. Ideally, 2DZM analysis of histology should occur beyond this division. For spherical objects, increasing the regularly spaced slice density is also effective for reducing form factor estimate error. The isotropic media simulations also indicated that as slice thickness increased, the objects appeared larger than they actually were. The rabbit liver study demonstrated the 2DZM method performing well using real

histology. Overall, the results suggest that 2DZMs are a feasible alternative to 3DZMs.

ACKNOWLEDGMENTS

The work was supported by National Institutes of Health (NIH) Grant No. R01-EB008992 and National Science Foundation (NSF) Grant No. CMMI-1300546. The authors would like to acknowledge the technical assistance of Alexander D. Pawlicki and Rita J. Miller, DVM (Doctor of Veterinary Medicine).

[1]S. I. Fields, "Ultrasound mammographic-histopathologic correlation," Ultrason. Imaging **2**, 150–161 (1980).
[2]R. C. Waag, J. Nilsson, and J. Astheimer, "Characterization of volume scattering power spectra in isotropic media from power spectra of scattering by planes," J. Acoust. Soc. Am. **74**, 1555–1571 (1983).
[3]M. F. Insana, "Modeling acoustic backscatter from kidney microstructure using an anisotropic correlation function," J. Acoust. Soc. Am. **97**, 649–655 (1995).
[4]G. Czarnota, M. Kolios, J. Abraham, M. Portnoy, F. Ottensmeyer, J. Hunt, and M. Sherar, "Ultrasound imaging of apoptosis: High-resolution non-invasive monitoring of programmed cell death *in vitro*, *in situ* and *in vivo*," Br. J. Cancer **81**, 520–527 (1999).
[5]J. Mamou, M. L. Oelze, W. D. O'Brien, Jr., and J. F. Zachary, "Identifying ultrasonic scattering sites from three-dimensional impedance maps," J. Acoust. Soc. Am. **117**, 413–423 (2005).
[6]J. Mamou, M. L. Oelze, W. D. O'Brien, Jr., and J. F. Zachary, "Extended three-dimensional impedance map methods for identifying ultrasonic scattering sites," J. Acoust. Soc. Am. **123**, 1195–1208 (2008).
[7]A. J. Dapore, M. R. King, J. Harter, S. Sarwate, M. L. Oelze, J. A. Zagzebski, M. N. Do, T. J. Hall, and W. D. O'Brien, Jr., "Analysis of human fibroadenomas using three-dimensional impedance maps," IEEE Trans. Med. Imaging **30**, 1206–1213 (2011).
[8]M. Gyöngy, L. Balogh, K. Szalai, and I. Kalló, "Histology-based simulations of ultrasound imaging: Methodology," Ultrasound Med. Biol. **39**, 1925–1929 (2013).
[9]P. M. Morse and K. U. Ingard, *Theoretical Acoustics* (McGraw-Hill, New York, 1968), pp. 400–463.
[10]M. Ueda and Y. Ozawa, "Spectral analysis of echoes for backscattering coefficient measurement," J. Acoust. Soc. Am. **77**, 38–47 (1985).
[11]M. F. Insana, R. F. Wagner, D. G. Brown, and T. J. Hall, "Describing small-scale structure in random media using pulse-echo ultrasound," J. Acoust. Soc. Am. **87**, 179–192 (1990).
[12]X. Chen, D. Phillips, K. Q. Schwarz, J. G. Mottley, and K. J. Parker, "The measurement of backscatter coefficient from a broadband pulse-echo system: A new formulation," IEEE Trans. Ultrason. Ferroelectr. Freq. Control **44**, 515–525 (1997).
[13]R. J. Lavarello, G. Ghoshal, and M. L. Oelze, "On the estimation of backscatter coefficients using single-element focused transducers," J. Acoust. Soc. Am. **129**, 2903–2911 (2011).
[14]M. F. Insana and D. G. Brown, "Acoustic scattering theory applied to soft biological tissues," in *Ultrasonic Scattering in Biological Tissues*, edited by K. K. Shung and G. A. Thieme (CRC, Boca Raton, FL, 1993), Chap. 4, pp. 76–124.
[15]A. M. Yaglom, *Correlation Theory of Stationary and Related Random Functions* (Springer, New York, 1987), pp. 348–361.
[16]R. Lavarello and M. Oelze, "Quantitative ultrasound estimates from populations of scatterers with continuous size distributions," IEEE Trans. Ultrason. Ferroelectr. Freq. Control **58**, 744–753 (2011).
[17]E. W. Montroll and R. W. Hart, "Scattering of plane waves by soft obstacles. II. Scattering by cylinders, spheroids, and disks," J. Appl. Phys. **22**, 1278–1289 (1951).
[18]A. Pawlicki, A. D. Dapore, S. Sarwate, and W. D. O'Brien, Jr., "Three-dimensional impedance map analysis of rabbit liver," J. Acoust. Soc. Am. **130**, EL334–EL338 (2011).